Measurement of B^0_d - $\overline{B}^0_d$ Oscillation Frequency Δm_d from the Time Evolution of $B^0 \to J/\psi K^*$

Matsubara Taro[1]

January 26, 2001

[1]matubara@hep.phys.s.u-tokyo.ac.jp

Abstract

This report describes measurement of the $B^0_d - \overline{B}^0_d$ oscillation frequency Δm_d in 5.8fb^{-1} data taken near the $\Upsilon(4S)$ resonance with the Belle detector at the KEK B-factory. Measurement of Δm_d is an essential ingredient for the measurement of indirect CP asymmetries. The decay mode $B^0 \to J/\psi K^*$ is used to reconstruct one B meson. The flavor of the accompanying B is identified mainly from the charges of leptons and kaons among its decay products. The time interval between the two B decays is determined from the distance between the decay vertex points. An unbinned maximum likelihood fit is performed to extract Δm_d. We obtain $\Delta m_d = 0.591 \pm 0.141(\mathrm{stat})^{+0.054}_{-0.112}(\mathrm{sys})$ ps^{-1}.

Contents

Chapter 1

Introduction

1.1 B^0_d - $\overline{B}^0_d$ Oscillation

The phenomenon of neutral particle-antiparticle oscillation is very general. As with the neutral kaon system, B^0 and $\overline{B}^0$ mesons mix with time evolution. The two physical eigenstates of neutral B mesons, B^0_H (heavy) and B^0_L (light), are linear combinations of the strong interaction eigenstates, B^0 and $\overline{B}^0$:

$$|B^0_H\rangle = p_B|B^0\rangle - q_B|\overline{B^0}\rangle, \quad (1.1)$$

$$|B^0_L\rangle = p_B|B^0\rangle + q_B|\overline{B^0}\rangle, \quad (1.2)$$

where p_B and p_B are normalized so that $|p^2_B| + |q^2_B| = 1$.

Applying the time-propagation operator to the mass eigenstates gives:

$$|B^0_H(t)\rangle = e^{-iM_Ht}e^{-\Gamma_Ht/2}|B^0_H\rangle = e^{-i(M_B+\Delta m_B)t}e^{-\Gamma_Bt/2}|B^0_H\rangle, \quad (1.3)$$

$$|B^0_L(t)\rangle = e^{-iM_Lt}e^{-\Gamma_Lt/2}|B^0_L\rangle = e^{-i(M_B-\Delta m_B)t}e^{-\Gamma_Bt/2}|B^0_L\rangle, \quad (1.4)$$

where M_H and M_L are the masses of B^0_H and B^0_L, respectively, M_B is their average, and Δm_B is their difference. Since the difference between the width of the two physical states is negligible ($\Delta\Gamma_B/\Gamma_B < 10^{-2}$), $\Delta\Gamma_B/\Gamma_B$ is approximated to be zero: $\Gamma_H = \Gamma_L = \Gamma_B$. As time increases, the amplitudes of these states decrease from decays and the phases change. However, a pure B^0_H state remains a pure B^0_H state and a pure B^0_L state remains a pure B^0_L state.

On the other hand, the B^0 state mixes with the $\overline{B}^0$ state. The time evolution of an initially pure B^0 states is expressed as;

$$|B^0(0)\rangle = \frac{1}{2p_B}(|B^0_H\rangle + |B^0_L\rangle), \quad (1.5)$$

$$|B^0(t)\rangle = \frac{1}{2p_B}e^{-iM_Bt}e^{-\frac{1}{2}\Gamma_Bt}\left\{e^{-\frac{i}{2}\Delta m_Bt}|B^0_H\rangle + e^{\frac{i}{2}\Delta m_Bt}|B_L\rangle\right\}$$

$$= e^{-iM_Bt}e^{-\frac{1}{2}\Gamma_Bt}\left\{\cos\left(\frac{1}{2}\Delta m_Bt\right)|B^0_H\rangle + \frac{iq_B}{p_B}\sin\left(\frac{1}{2}\Delta m_Bt\right)|B_L\rangle\right\}. \quad (1.6)$$

Since q_B/p_B has been measured to be consistent to be one, the probabilities for the initial state $|B^0\rangle$ to become the final state $|B^0\rangle$ and $|\overline{B^0}\rangle$ are

$$P(B^0 \to B^0) = |\langle B^0|B^0(t)\rangle|^2 = \frac{1}{2}e^{-\Gamma_B t}[1+\cos(\Delta m_B t)], \quad (1.7)$$

$$P(B^0 \to \overline{B}^0) = |\langle \overline{B^0}|B^0(t)\rangle|^2 = \frac{1}{2}e^{-\Gamma_B t}[1-\cos(\Delta m_B t)], \quad (1.8)$$

The same relations can be shown in the case of an initially pure $\overline{B}^0$ state.

The mass difference for B_d^0, Δm_d, can be represented by the CKM (Cabibbo-Kobayashi-Maskawa) matrix element, V_{td}. The Lagrangian of the charged current interaction in terms of the mass eigenstates forms

$$\mathcal{L}_W = -\frac{g}{\sqrt{2}}(\overline{u}_L, \overline{c}_L, \overline{t}_L)\gamma^\mu V \begin{pmatrix} d_L \\ s_L \\ b_L \end{pmatrix} W_\mu^+ + h.c., \quad (1.9)$$

where the CKM matrix V is a unitary matrix in the flavor space. For the case of three generations, V is, then, explicitly written as;

$$V = \begin{pmatrix} V_{ud} & V_{us} & V_{ub} \\ V_{cd} & V_{cs} & V_{cb} \\ V_{td} & V_{ts} & V_{tb} \end{pmatrix}. \quad (1.10)$$

The diagrams in Figure 1.1 display the main interaction which lead to B_d^0 - $\overline{B}_d^0$ mixing. The interaction is completely dominated by intermediate t-quarks. Evaluation of these diagrams leads to the following formula for the oscillation frequency:

$$\Delta m_d = \frac{G_F^2}{6\pi^2}|V_{td}V_{tb}^*|^2 m_t^2 m_{B_d} f_B^2 B_B \eta_{QCD} F\left(\frac{m_t^2}{m_W^2}\right), \quad (1.11)$$

where G_F is the Fermi coupling constant, V_{td} and V_{tb} are the CKM-matrix elements, f_B is the decay constant, B_B is the bag parameter of B meson, η_{QCD} is QCD correction, and m_t (m_W) is the top quark mass (W boson mass). Currently, uncertainties on f_B, B_B and η_{QCD} limit the prediction accuracy of V_{td}. The oscillation frequency Δm_d is proportional to the square of $|V_{td}V_{tb}^*|$. Accurate measurements of Δm_d provide a mathematical constraint on unitarity of the CKM matrix.

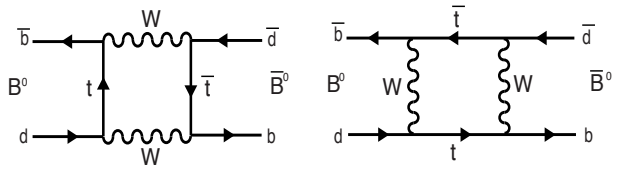

Figure 1.1: The box diagrams for neutral B meson mixing

1.2 Studying B^0_d - $\overline{B}^0_d$ Oscillation at KEKB

We study B^0_d-$\overline{B}^0_d$ oscillation using the data collected at the B-factory of High Energy Accelerator Research organization (KEK). The primary goal of KEK B-factory project is to establish the CP violation in B decays.

The measurement of B^0_d - $\overline{B}^0_d$ oscillation is an essential demonstration for ability to measure the indirect CP violation at Belle, which is the main purpose of the experiment. CP violation is the key to understand the puzzling fact that the universe is made of matter, not of anti-matter. However, the mechanism of CP violation has not been understood perfectly. Indirect CP violation occurs through B^0_d-$\overline{B}^0_d$ oscillation, and it appears as a difference of oscillation between B^0_d and $\overline{B}^0_d$ mesons.

LEP (Large Electron Positron Collider) and CDF (Collider Detector at Fermilab) experiments have measured Δm_d. KEK B-factory (KEKB) has several advantages for the Δm_d measurement. One of the advantages is large statistics. KEKB is designed to produce large quantity of $B^0\overline{B}^0$ pairs, typically about $10^7 \sim 10^8$, in order to observe and study CP violation in the B meson system in detail. KEKB provided the integrated luminosity of 6.2fb^{-1} in the first year of operation. Another advantage is smaller number of background events. Ratio of signal to background events is 1/3 at KEKB while it is 10^{-4} at CDF. $\Delta m_d = 0.463 \pm 0.008(\text{stat}) \pm 0.016(\text{sys})$ ps^{-1} is obtained from the time evolution of dilepton events at the Υ(4S) at Belle[2], which is consistent with the world average value: $\Delta m_d = 0.472 \pm 0.017$ ps^{-1}[3].

We determine Δm_d from the time evolution of opposite flavor ($B^0_d\overline{B}^0_d$) and same flavor ($B^0_dB^0_d$, $\overline{B}^0_d\overline{B}^0_d$) decay pairs in $\Upsilon(4S)$ decays. The time dependent probabilities of observing opposite flavor (P_{OF}) and same flavor (P_{SF}) states are given by

$$P_{OF}(\Delta t) = \frac{1}{4\tau_{B^0}} \exp\left(-\frac{\Delta t}{\tau_{B^0}}\right)[1 + \cos(\Delta m_d \Delta t)], \tag{1.12}$$

$$P_{SF}(\Delta t) = \frac{1}{4\tau_{B^0}} \exp\left(-\frac{\Delta t}{\tau_{B^0}}\right)[1 - \cos(\Delta m_d \Delta t)], \tag{1.13}$$

where τ_{B^0} is the average neutral B meson lifetime, and Δt is the proper time difference between the two B^0 meson decays. KEKB employs an 8.0 GeV electron beam and a 3.5 GeV positron beam, resulting in a center of mass moving along the electron beam direction with a Lorentz boost of $\beta\gamma = 0.425$. The proper time difference Δt can be approximated as

$$\Delta t \simeq \Delta z / c\beta\gamma, \tag{1.14}$$

where Δz is the distance between the decay vertices of the two B mesons along the beam direction. The decay vertices of the two B mesons are typically separated by 200 μm. The Belle detector is required to have a resolution better than $\tau_{B^0}/2$, corresponding to a Δz resolution of 100 μm.

In this thesis, B^0_d - $\overline{B}^0_d$ oscillation frequency Δm_d is measured using the following decay chain (charge conjugate modes are implied throughout this paper),

$$B^0_d \to J/\psi K^{*0},\ K^{*0} \to K^+\pi^-,\ J/\psi \to \ell^+\ell^-\ (\ell = e, \mu).$$

The Feynman diagram of $B^0_d \to J/\psi K^{*0}$ is shown in Figure 1.2. Invariant mass, the beam constrained mass and the energy difference between the energy of the neutral B candidate and beam energy are calculated to reconstruct the B mesons.

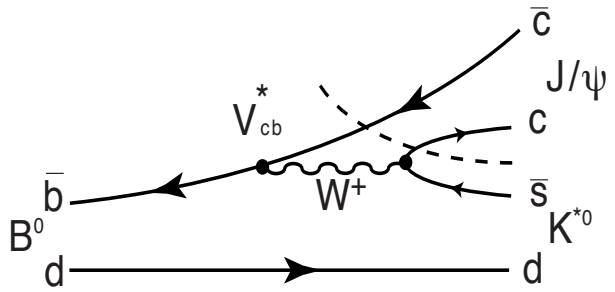

Figure 1.2: Feynman diagram for $B^0_d \to J/\psi K^{*0}$. The dashed line separates the hadronic currents.

The observation of B^0_d - $\overline{B}^0_d$ oscillation and the measurement of the oscillation frequency, Δm_d, require precise identification of the flavor of the B meson. The flavor of the neutral B^0 meson reconstructed from $B^0_d \to J/\psi K^{*0}$ can be determined from the charge of the kaon. The flavor of associated B^0 meson is identifed using the correlation between the flavor and the charge of the daughter particles, mainly kaons and leptons. The Belle detector is also required to have a good particle identification capability in order to determine B meson flavors.

The analysis presented here is based on integrated luminosity of 5.8 fb^{-1} on the $\Upsilon(4S)$ resonance. The outline of this thesis is as follows: An overview of the KEKB accelerator and the Belle detector is described in Chapter 2. In Chapter 3, we describe the analysis procedure to measure the oscillation frequency Δm_d using the Monte Carlo simulation sample. In Chapter 4, Δm_d is extracted from the real data based on the method described in Chapter 3. Chapter 5 concludes the analysis result.

Chapter 2

B-factory Experiment

In this chapter we describe the Belle detector and the KEKB accelerator.

The Belle detector is designed to observe and measure CP violation in B decays. Because of the high luminosity of KEK B-factory ($\mathcal{L}_{peak} \approx 2 \times 10^{33}$ cm^{-2}s^{-1}), Belle currently accumulates data at a rate of more than 1.5 fb^{-1} per month. This corresponds to 1.6 million $B\overline{B}$ events per month, allowing precise measurements of B meson properties. Due to the asymmetric energies of the colliding beams, the $\Upsilon(4S)$ and its daughter B mesons are produced at $\beta\gamma \sim 0.425$ in the laboratory flame: the difference in B meson decay times can be measured using the difference in the decay vertex positions. This key feature of the Belle experiment allows the measurement of CP violation through oscillation in neutral B decays, if it occurs.

In Section 2.1, a brief introduction of the KEKB accelerator is given. In Section 2.2, the overview of the Belle detector and the description of its principal components are given.

2.1 KEKB Accelerator

The configuration of the KEKB accelerator is shown in Figure 2.1. B mesons must be boosted to measure the decay time difference of B and $\overline{B}$ mesons. In order to boost B meson pairs, the KEKB is designed to be an asymmetric electron-positron collider. The energies of electrons and positrons are 8 GeV and 3.5 GeV, respectively. The center-of-mass energy is 10.58 GeV, which corresponds to $\Upsilon(4S)$ resonance. Electrons have higher energy than positrons in order to avoid ion trapping, which happens at low energies. The design luminosity is 10^{34} cm^{-2}s^{-1} to produce 10^8 $\Upsilon(4S)$ a year.

Electron and positron rings are built side by side in the existing TRISTAN tunnel, which has a circumference of about 3 km. KEKB has only one interaction point (IP) in the Tsukuba experimental hall, where the electron and positron beams collide at a finite angle of 22 mrad to avoid parasitic collision. The Belle detector is installed in this interaction region.

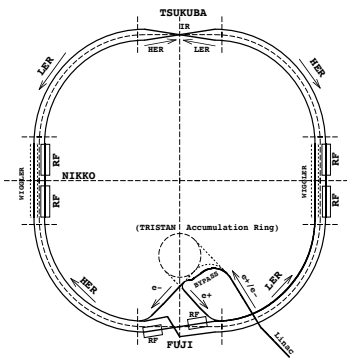

Figure 2.1: Configuration of the KEKB accelerator system

2.2 Belle Detector

The configuration of the Belle detector is shown in Figure 2.2. Because of

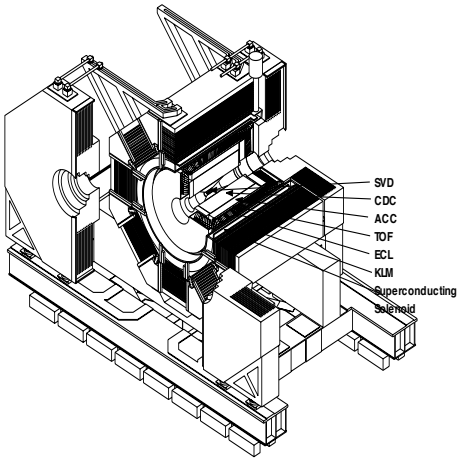

Figure 2.2: Schematic view of the Belle detector

the asymmetry of the beam energies, the detector itself is asymmetric: *i.e.* it has a larger acceptance in the detection of electrons (which is defined as "the forward region"). B meson decay vertices are measured by the Silicon Vertex Detector (SVD) just outside a cylindrical beryllium beam pipe. Charged particle tracking is provided by the Central Drift Chamber (CDC). Particle identification is provided by dE/dx measurement in the CDC and the Aerogel Čerenkov Counter (ACC) and the Time of Flight (TOF) counter arrays outside the CDC. Electromagnetic showers are detected in the CsI(Tℓ) Electromagnetic

Calorimeter (ECL) located inside the superconducting solenoid, which provides magnetic field of 1.5 Tesla. The K_L mesons and muon counters (KLM), which consist of resistive plate counters (RPCs), are interspersed in the iron return yoke of the magnet. A brief description of each component follows.

2.2.1 Silicon Vertex Detector (SVD)

The main task of the Silicon Vertex Detector (SVD) is to reconstruct the decay vertices of two primary B mesons in order to determine the time difference between two decays. It is required to achieve $\Delta t/\tau_B \leq 0.5$ for CP violation measurement, corresponding to about 100 μm position resolution in the beam direction. Intrinsic resolution of SSD (Silicon Strip Detector) is expected to be a few tens of microns, which is much better than the resolution of a wire drift chamber.

The tracks produced at the KEKB are rather soft and multiple-Coulomb scattering is a dominant source of the vertex resolution degradation. This imposes strict constraints on the detector design and mechanical layout. The innermost layer of the support structure must be low mass but stiff; and the readout electronics must be placed outside of the tracking volume.

The SVD has three cylindrical layers consisting of units of the silicon sensors. The SVD is not required to function as a stand-alone tracker for low p_T tracks since the CDC can reconstruct low momentum tracks down to p_T of about 70 MeV/c. The position of each layer is 3.0 cm, 4.55 cm and 6.05 cm in r direction, respectively. The SVD covers $23^\circ < \theta < 139^\circ$, corresponding to the angular acceptance of 86% of 4π. The three layers have 8, 10 and 14 sensor ladders in ϕ. The structure of SVD is shown in Figure 2.3.

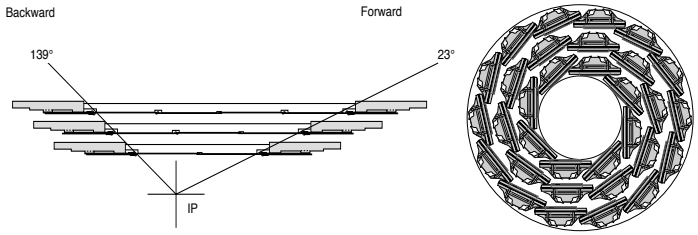

(a) Side view (b) End view

Figure 2.3: Side and end views of the Belle SVD

Each layer is constructed from double-sided silicon strip detectors (DSSDs) and the front end electronics. We use the S6939 DSSDs fabricated by HAMAMATSU Photonics. One side (= n-side) of DSSDs has n^+-strips oriented perpendicular to the beam direction to measure the z coordinate and the other side (= p-side) with longitudinal p^+-strips for ϕ coordinate measurement. The

z strip pitch is 42 μm and the ϕ strip pitch is 25 μm. Adjacent strips are connected to one readout trace on the z-side which gives an effective strip pitch of 84 μm. Every other sense-strip is connected to read-out electronics on the ϕ-side. Signals collected by floating strips are read out from adjacent strips by means of capacitive charge division. In total 102 DSSDs are used and the total number of readout channels is 81920. The bias voltage of 80 V is supplied to the n-side and p-side is grounded.

We use the VA1 chips manufactured by IDE AS in Norway as the readout LSI for the DSSDs, because of good radiation tolerance. The VA1 chip consists of 128-channel pre-amplifiers, shapers, sample/hold circuits and analog multiplier.

The impact parameter resolutions for 2 track events obtained from collision data and cosmic data in $r\phi$ plane and along the z is shown in Figure 2.4. The resolutions are

$$\sigma_{r\phi}^2 = (19)^2 + \left(\frac{50}{p\beta\sin^{3/2}\theta}\right)^2 \mu\mathrm{m}^2, \quad \sigma_z^2 = (36)^2 + \left(\frac{42}{p\beta\sin^{5/2}\theta}\right)^2 \mu\mathrm{m}^2, \quad (2.1)$$

respectively, where p is the charged track momentum measured in GeV/c, β is the velocity divided by c, and θ is the angle from the beam axis.

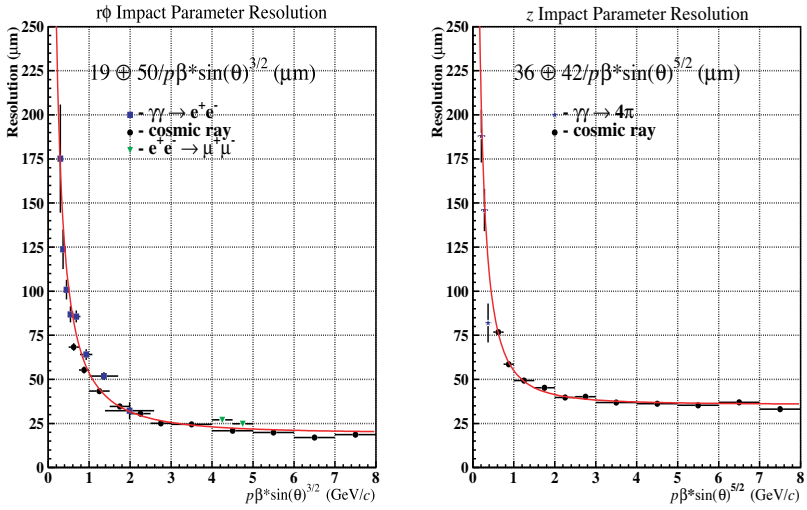

(a) $r\phi$ resolution

(b) z resolution

Figure 2.4: The impact parameter resolution of the Belle SVD

2.2.2 Central Drift Chamber (CDC)

The main role of the Central Drift Chamber (CDC) is the detection of charged particles. The structure of the CDC is shown in Figure 2.5. Specifically, the physics goals of the Belle experiment require a momentum resolution better than $\sigma_{p_T}/p_T \sim 0.25 \cdot \sqrt{1+p_T^2}$ % for all charged particles with $p_T \geq 100$ MeV/c, where p_T is the transverse momentum. In addition, the CDC is expected to provide particle identification information in the form of precise dE/dx measurement for charged particles.

The CDC covers $17^\circ \leq \theta \leq 150^\circ$, providing angular acceptance of 92% of 4π in the $\Upsilon(4S)$ rest frame. The inner and outer radii are 9 cm and 88 cm, respectively. The CDC consists of 50 sense wire layers in total and 3 cathode strip layers. The sense-wire layers are grouped into 11 superlayers, where 6 of them are axial and 5 are stereo super layers. The number of readout channels is 8,400 for anode wires and 1,792 for cathode strips. 50% Helium - 50% ethane (C_2H_6) gas mixture is filled in the chamber to minimize the multiple-Coulomb scattering. A magnetic field of 1.5 Tesla is chosen to minimize momentum resolution without sacrificing efficiency for low momentum tracks.

From the result of the beam test, the overall spatial resolution is 130μm and the transverse momentum resolution is $(\sigma_{p_T}/p_T)^2 = (0.0019 p_T)^2 + (0.0034)^2$, where p_T is the transverse momentum measured in GeV/c. The dE/dx measurements have a resolution for hadron tracks of $\sigma(dE/dx) = 6.9\%$ and are useful for 3σ K/π separation below 0.8 GeV/c. The CDC is also useful for 4σ e/π separation. e/π separation below 1 GeV/c is very important for electron identification because the e/π identification using the ECL is not effective in this momentum region.

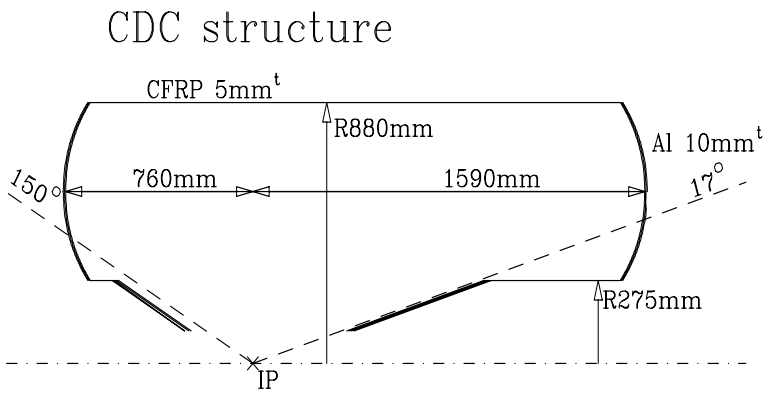

Figure 2.5: Structure of the Central Drift Chamber

2.2.3 Aerogel Čerenkov Counter (ACC)

The Aerogel Čerenkov Counter (ACC) system extends the coverage for particle identification from the momentum $p \geq 1.2$ GeV/c, the upper limit of the Time of Flight system, to the kinematic limit of 2-body B decays such as $B^0 \to \pi^+\pi^-$, *i.e.* $p = 2.5$ GeV/$c \sim 3.5$ GeV/c, depending on the polar angle.

The Aerogel of the ACC is SiO_2. The reflection index of the aerogel is chosen so that the pion produces Čerenkov light in the aerogel while the kaon does not. In general, the threshold of the Čerenkov light emission in the matter with the reflective index of n is represented using the velocity of particle β as;

$$n > 1/\beta = \sqrt{1 + (m/p)^2}, \tag{2.2}$$

where the particle momentum p is measured by the CDC.

Each aerogel counter module consists of silica aerogel radiator module and fine-mesh photo multiplier tubes to detect Čerenkov radiation. The typical aerogel module comprises aerogel tiles contained in a 0.2-mm-thick aluminum box.

The ACC is divided into two part. A barrel array (BACC) covers an angular range of $34° < \theta < 127°$ and a forward end-cap array (EACC) covers an angular range of $17° < \theta < 34°$.

The BACC provides 3σ K/π separation in the momentum region 1.0 GeV/c $< p_K <$ 3.6 GeV/c. The BACC consists of 960 aerogel counter modules. Five different indices of reflection, $n = 1.01$, 1.013, 1.015, 1.020 and 1.028 are used depending on the polar angle. Each barrel counter is viewed by one or two fine-mesh photo-multipliers.

The EACC consists of 288 modules of which the reflection index equals to 1.03. This eliminates the need for the TOF system in end-cap region, since this reflection index gives 3σ K/π separation in the momentum range from 0.7 GeV/c to 2.4 GeV/c. This approach provides complete endcap flavor tagging, as well as particle identification for many of the few-body decays relevant to CP eigenstates.

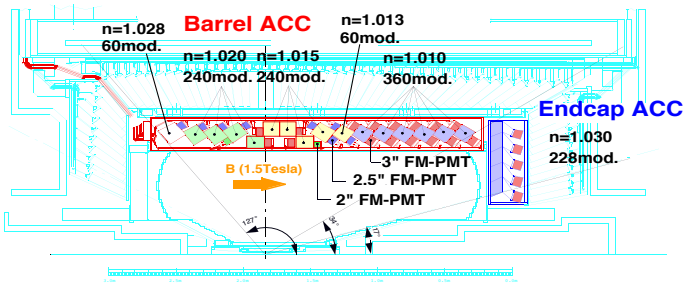

Figure 2.6: The configuration of the ACC

2.2.4 Time/Trigger of Flight Counter (TOF)

The Time of Flight counter (TOF) system is required to have a 100 ps time resolution in order to provide 3σ K/π separation for momenta below 1.2 GeV/c, the region of interest for B flavor tagging.

The relation between the measured flight time T and the particle momentum p measured by the CDC is expressed as;

$$T = \frac{L}{c}\sqrt{1 + (m/p)^2}, \tag{2.3}$$

where L is the flight length depends on the TOF geometry and m is the particle mass. Because of the mass difference between kaons and pions, the difference of T between kaons and pions is $\sim$ 300 ps at $p = 1.2$ GeV/c. The TOF has a time resolution of 95 ps and provides 3σ K/π separation.

The TOF system comprises 64 barrel TOF/Trigger Scintillation Counter (TSC) modules. A TOF/TSC module consists of two trapezoid shaped 4-cm-thick counters and one 5-mm-thick TSC counter separated by a 2-cm gap as shown in Figure 2.7. A coincidence between TSC and TOF counters rejects γ background and provides a clean event timing to the Belle trigger system.

The TOF is segmented into 128 in ϕ sectors and readout by one FM-PMT at each end. TSCs have 64-fold segmentation and are readout from only backward end by a single FM-PMT. The number of readout channels is 256 for the TOF and 64 for the TSC. Each module is located at $r = 120$ cm. The TOF/TSC system covers an angle range of $34° < \theta < 121°$.

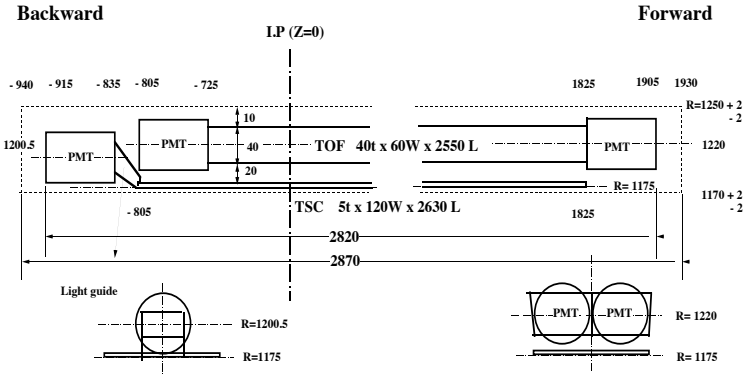

Figure 2.7: The configuration of the TOF/TSC

2.2.5 Electromagnetic Calorimeter (ECL)

The main purpose of the Electromagnetic Calorimeter (ECL) is the detection of electromagnetic shower caused by photons and electrons from B meson decays with high efficiency and good energy resolution.

Most of the physics goals of the Belle experiment require reconstruction of exclusive B meson final states. For typical B meson decay approximately one third of the final state particles are π^0's, thus it is important to have photon detection capabilities that match those for charged particles, especially for low energy photons. π^0 mass resolution is dominated by the photon energy resolution. Sensitivity to and resolution of low energy photons are the critical parameters for the efficient π^0 detection.

Electron identification in the Belle relies primarily on a comparison to the charged particle track momentum and the energy it deposits in the electromagnetic calorimeter. Good energy resolution of the calorimeter results in better hadron rejection.

In order to satisfy these requirements, we choose a design of the electromagnetic calorimeter based on CsI (Tℓ) crystal. All CsI (Tℓ) crystals are 30 cm (16.1 radiation length) long, and are assembled into a tower structure pointing near the interaction point. The barrel part of the ECL has 46-fold segmentation in θ and 144-fold segmentation in ϕ.

The forward (backward) endcap part of the ECL has 13-(10-)fold segmentation in θ and the ϕ segmentation varies from 48 to 144 (64 to 144). The barrel part has 6,624 crystals and the forward (backward) endcap part has 1,153 (960) crystals. Each crystal is readout by two 10×20 mm^2 photo-diodes. Total readout channel is 17,472. The inner radius of the barrel part is 125 cm. The forward (backward) endcap part starts at $z = +196$ cm (-102 cm).

The ECL has the photon energy resolution $\sigma_E/E = (0.013)^2 + (0.0007/E)^2 + (0.008/E^{1/4})^2$, where E is measured in GeV. Neutral pions are detected via their decay to $\gamma\gamma$. The π^0 mass resolution varies slightly with energy, averaging $\sigma_{m_{\pi^0}} = 4.9$ MeV/c^2. With a 3σ mass selection requirement, the overall π^0 detection efficiency from $B\overline{B}$ events, including geometric acceptance, is 40%.

2.2.6 Solenoid Magnet

The magnetic field causes a charged particle to follow a helical path. Its curvature is related to the momentum of the particles. The coil consists of a single layer of an aluminum-stabilized superconductor coil, a niobium-titanium-copper alloy embedded in a high purity aluminum stabilizer. It is wound around the inner surface of an aluminum support cylinder. Indirect cooling is provided by liquid helium circulating through a single tube welded on the outer surface of the support structure. The superconducting solenoid magnet provides a magnetic field strength of 1.5 Tesla in a cylindrical volume of 3.4 m in diameter and 4.4 m in length. The field value in the CDC volume is expected to vary by 2.0%.

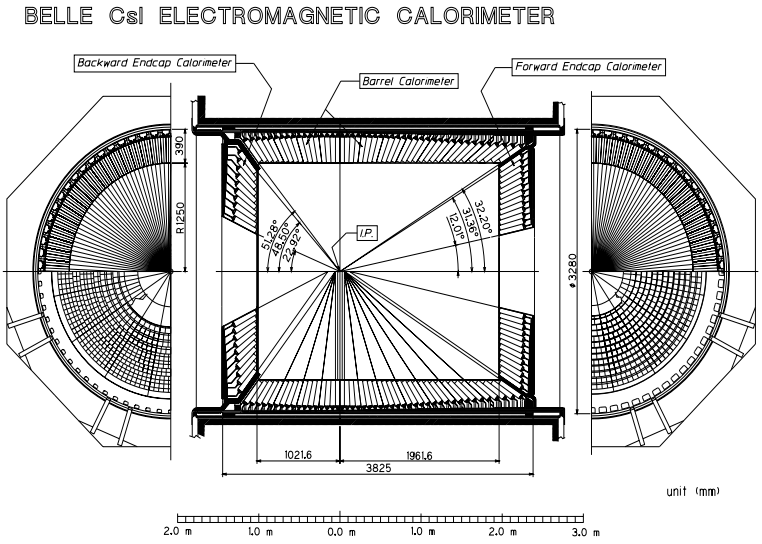

Figure 2.8: The configuration of the Electromagnetic Calorimeter

2.2.7 K_L and Muon Detector (KLM)

The K_L and Muon Detector (KLM) is designed to detect neutral kaons and muons with momenta above 600 MeV/c. The detection of K_L is needed to reconstruct $B \to J/\psi K_L$. Muons are used in the CP violation measurements to identify the flavor of B meson and to reconstruct $J/\psi \to \mu^+\mu^-$.

Resistive Plate Counter (RPC) is utilized for the Belle KLM system. RPC's are essentially planar spark counters wherein the avalanche induced by an incident charged particle is quenched when the limited amount of charge on the inner surfaces of highly resistive electrodes is exhausted. Having a particle penetrating an RPC, it becomes locally deadend for short time until the inner surfaces can recharge through the resistive material. The Belle KLM employs glass as resistive material for RPC, which has a bulk resistivity of about $10^{12} \sim 10^{13}$ Ωcm.

The KLM detector consists of a barrel part and two endcap parts. Fourteen layers are 4.7 cm thick iron plates and each RPC superlayer contains two RPC planes and provides θ and ϕ information. The barrel part has one additional RPC superlayer in front of the first iron plate. RPC is made of 2-mm thick glass electrodes. The iron plate is an absorber material for the KLM and also serves as a return path of the magnetic flux provided by solenoid magnet. K_L is tagged with hadronic interactions in the ECL, the coil or the KLM itself. Nominally, the detector covers the polar angle range of $25° < \theta < 145°$. Signals are readout by $\sim$ 5 cm wide cathode strips in both θ and ϕ. The number of readout channels is 32,856 in barrel and 16,128 in endcap.

The overall muon identification efficiency is above 90% for $p > 1$ GeV/c tracks detected in the CDC. The probability that pion is misidentified as muon

is below 2%. K_L mesons are identified by the presence of KLM hits originating from hadronic interactions of the K_L in the CsI and/or iron. The angular resolution of the K_L direction is estimated to be $\sim 1.5^\circ$ and $\sim 3^\circ$ with and without associated CsI hits.

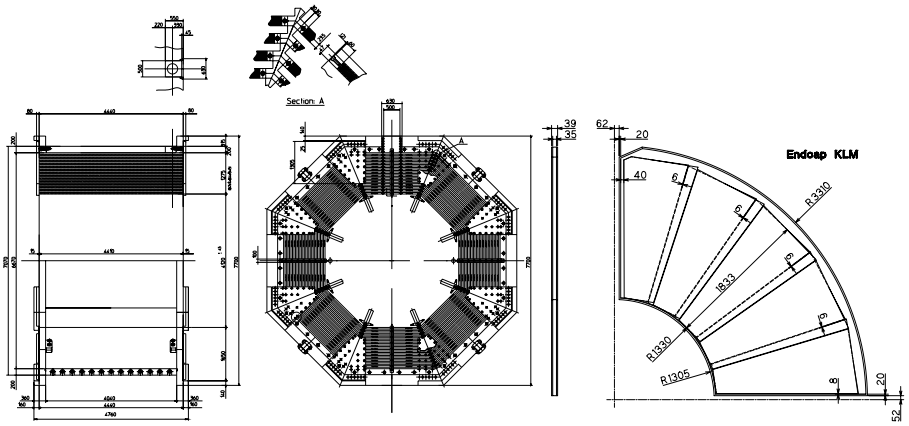

(a) Barrel part (b) Endcap part

Figure 2.9: The barrel and endcap parts of the Belle KLM

Chapter 3

Measurement of the Oscillation Frequency Δm_d

3.1 Overview

We give a brief overview of the analysis procedure to observe the B^0_d-$\overline{B}^0_d$ oscillation at the Belle experiment in this section. Detailed description of each process is given in the following sections.

We reconstruct $B^0 \to J/\psi K^{*0}$ mode to separate the daughter tracks of one B^0 meson from the tracks of the other B^0 meson. We select this mode because of its small background. J/ψ candidates are identified via $J/\psi \to e^+e^-$ or $J/\psi \to \mu^+\mu^-$ and K^{*0} candidates are identified via $K^{*0} \to K^+\pi^-$. The J/ψ and K^{*0} candidates are selected based on the invariant mass calculated from energies and momenta of the daughter tracks. B^0 candidates are selected based on the beam constrained mass and the energy difference between the energy of the B^0 candidate and beam energy, which are explained in the following section.

The flavor of the reconstructed B meson is identified from the charge of the K meson. The flavor of the associated B^0 meson is identified using the correlation between the flavor and the charge of the daughter particles. Decay chain of the associated B^0 meson is not reconstructed to avoid efficiency loss.

We obtain the B^0 decay vertices using the lepton tracks from $J/\psi \to \ell^+\ell^-$ decay, because lifetime of J/ψ is very short and its decay vertex can be treated as B decay vertex. The decay vertex of the associated B^0 meson is obtained using the remaining charged tracks. The proper time difference Δt is approximated using the distance between the decay vertices of the two B mesons along the beam direction (Δz) as

$$\Delta t \simeq \Delta z / c\beta\gamma, \tag{3.1}$$

where $\beta\gamma$ is the Lorentz boost factor due to the asymmetric beam energy. The flight distance perpendicular to the beam direction can be ignored because the B meson momentum is small (~ 300 MeV/c) in the center-of-mass frame of the $\Upsilon(4S)$ resonance.

Δm_d is derived from the Δt dependence of the B^0_d-$\overline{B}^0_d$ mixing. Here we classify an event according to the flavor of the two B mesons as;

- Same Flavor (SF): both B mesons have same flavor.
- Opposite Flavor (OF): both B mesons have opposite flavor.

The probability to observe an OF or SF event is given by

$$P_{OF}(\Delta t) = \frac{1}{4\tau_{B^0}} \exp\left(-\frac{|\Delta t|}{\tau_{B^0}}\right)[1+\cos(\Delta m_d \Delta t)], \tag{3.2}$$

$$P_{SF}(\Delta t) = \frac{1}{4\tau_{B^0}} \exp\left(-\frac{|\Delta t|}{\tau_{B^0}}\right)[1-\cos(\Delta m_d \Delta t)], \tag{3.3}$$

where τ_{B^0} is B^0 lifetime and Δm_d is the mass difference of the two mass eigenstates, $\Delta m_d = m_{B^0_H} - m_{B^0_L}$, which appears as the oscillation frequency of B^0_d-$\overline{B}^0_d$ mixing. An unbinned maximum likelihood fit is performed to extract Δm_d from the Δt distributions of OF and SF events.

Monte Carlo events corresponding to 50 fb^{-1} are generated with τ_{B^0} = 1.56 ps and $\Delta m_d = 0.423$ ps^{-1} to study the selection of B^0 candidates, the proper time calculation, and the fit procedure to extract Δm_d . The Monte Carlo sample includes all physics events including background events generated at the energy of $\Upsilon(4S)$ resonance.

3.2 Event Selection

Hadronic events are selected using the selection criteria as follows. Radical component of the primary event vertex should be less than 1.5 cm and z component should be within $\pm$3.5 cm to reject beam-wall and beam-gas events. The number of charged tracks with good quality should be greater than or equal to 5 to achieve high spatial resolution. Total visible energy calculated in the the $\Upsilon(4S)$ rest frame should be greater than or equal to 50% of the center of mass energy. Absolute value of z component sum for charged track momenta and cluster energies in the $\Upsilon(4S)$ rest frame should be between 2.5% and 90% of the center of mass energy. These cuts are applied to eliminate Bhabha, $\mu^+\mu^-$, and other background events.

Ratio of 2nd to 0th Fox-Wolfram moments R_2 is used to reject continuum events. The R_2 is defined as a ratio

$$R_2 = H_2/H_0, \tag{3.4}$$

where the ith Fox-Wolfram moment H_i is defined as

$$H_i \equiv \sum_{j,k} \frac{|\overrightarrow{p_j}||\overrightarrow{p_k}|}{E^2} P_i(\cos\phi_{jk}), \tag{3.5}$$

where the indices j,k run over all tracks in the event, $\overrightarrow{p_j}$ is the momentum of the track j in the $\Upsilon(4S)$ rest frame, E is the total energy of the event in the

$\Upsilon(4S)$ rest frame, ϕ_{jk} is the angle between the track j and k, and $P_i(x)$ is the ith Legendre polynomial. R_2 is close to 0 for $B\overline{B}$ events, while R_2 is close to 1 for jet-like continuum events. The distributions for R_2 of $B\overline{B}$ events and continuum events are shown in Figure 3.1. We accept events with R_2 less than 0.4. This cut eliminates more than 40% of continuum events, while retaining more than 99% of $B\overline{B}$ events.

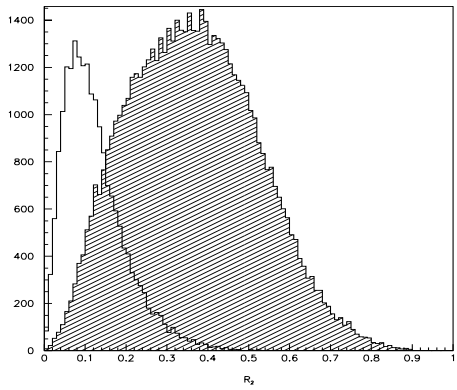

Figure 3.1: The R_2 distributions for the MC sample. Solid line shows the R_2 distribution for $B\overline{B}$ events. Hatched area shows the R_2 distribution for continuum events.

3.3 Event Reconstruction

In this study, one B^0 meson is identified by reconstructing $B^0 \to J/\psi K^{*0}$, $J/\psi \to \ell^+\ell^-$, $K^{*0} \to K^+\pi^-$ decay chain. Total branching fraction of this decay chain is $(1.35 \times 10^{-3}) \times 0.12 \times 2/3 \simeq 1.1 \times 10^{-4}$. The properties of the particles used in this analysis are tabulated in Table 3.1.

	Mass [MeV]	Lifetime	J	I
B^0	5279.4 ± 0.5	$(1.548 \pm 0.032) \times 10^{-12}$s	0	1/2
J/ψ	3096.87 ± 0.04	$(7.6 \pm 0.4) \times 10^{-21}$s	1	0
K^{*0}	896.10 ± 0.27	$(1.30 \pm 0.02) \times 10^{-23}$s	1	1/2
$K^{\pm}$	493.677 ± 0.016	$(1.2386 \pm 0.0024) \times 10^{-8}$s	0	1/2
$\pi^{\pm}$	139.57018 ± 0.00035	$(2.6033 \pm 0.0005) \times 10^{-8}$s	0	
$e^{\pm}$	$0.510998902 \pm 0.00000021$	$> 4.2 \times 10^{23}$y	1/2	
$\mu^{\pm}$	105.658357 ± 0.000005	$(2.19703 \pm 0.00004) \times 10^{-6}$s	1/2	

Table 3.1: The properties of the particles used in this analysis[3]

3.3.1 Reconstruction of J/ψ

J/ψ is identified using dilepton decays: $J/\psi \to e^+e^-$ and $J/\psi \to \mu^+\mu^-$. The branching fractions of J/ψ decay to lepton pair are tabulated in Table 3.2.

J/ψ decay mode	Branching fraction of J/ψ decay
$J/\psi \to e^+e^-$	$(5.93 \pm 0.10) \times 10^{-2}$
$J/\psi \to \mu^+\mu^-$	$(5.88 \pm 0.10) \times 10^{-2}$

Table 3.2: The Branching fractions of J/ψ decays[3]

Electrons and positrons are identified by combining information from several detectors such as the matching between the energy measured in the ECL, the momentum measured in the CDC, the shower shape of the cluster energy deposit in the ECL, and dE/dx measured in the CDC. The electron likelihood is calculated from these measurements and it is required to be consistent with electrons. If there is an energy cluster in the ECL within 0.05 radians of the identified track, its energy is added to that of the track to take into account photons emitted by radiative decay of J/ψ. The invariant mass of two tracks, both of which satisfy the criteria above and have the opposite charges, is calculated. The track pair is identified as a $J/\psi \to e^+e^-$ if the mass lies in the range $2.947\ \mathrm{GeV}/c^2 < M(e^+e^-) < 3.133\ \mathrm{GeV}/c^2$.

Muons are identified based on the information from the associated hits in the KLM. The number of hit layers in the KLM is compared with the expected number calculated from the momentum measured in the CDC. The energy deposit in the ECL should be consistent with minimum ionizing. The muon likelihood is calculated by combining the KLM and ECL information. A track whose likelihood is consistent with that of a muon is identified as a muon track. The dimuon invariant mass is required to lie in the range $3.037\mathrm{GeV}/c^2 < M(\mu^+\mu^-) < 3.133\ \mathrm{GeV}/c^2$ to be identified as a J/ψ. The dilepton invariant mass distributions for the MC sample are shown in Figure 3.2. A kinematic fit with the J/ψ mass constraint is performed on the J/ψ candidate to improve the resolution.

3.3.2 Reconstruction of K^{*0}

The K^{*0} candidates are reconstructed using the decay mode $K^{*0} \to K^+\pi^-$. Charged kaons are identified by requiring that the kaon likelihood of a track is greater than pion likelihood. The kaon likelihood is obtained by combining the time of flight measured in the TOF, dE/dx and hit information measured in the ACC. The tracks which are identified as neither kaons nor leptons in the J/ψ reconstruction are treated as charged pion candidates.

A K^{*0} candidate is identified if the invariant mass of a kaon-pion pair is within 75 MeV/c^2 of the nominal K^{*0} mass. Figure 3.3 shows the invariant mass distribution for K^{*0} candidates in the MC sample.

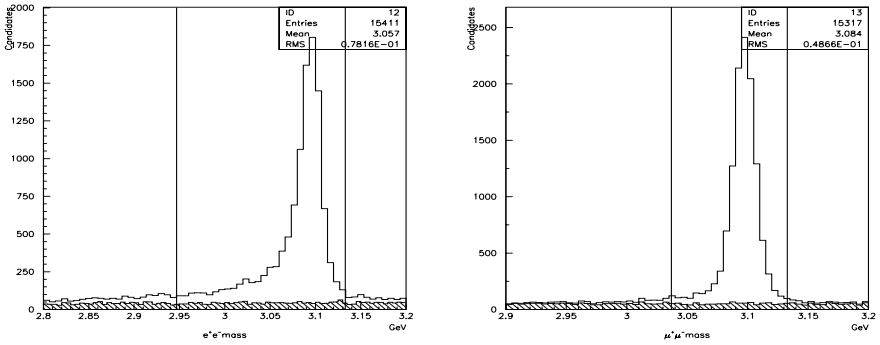

(a) $J/\psi \to e^+e^-$ (b) $J/\psi \to \mu^+\mu^-$

Figure 3.2: Invariant mass distributions for J/ψ candidates in the MC sample. Hatched area shows the background distribution. Selection criteria are indicated by straight lines.

3.3.3 Reconstruction of B^0

B^0 candidates are reconstructed from J/ψ and K^{*0}. Figure 3.4 shows the invariant mass distribution of J/ψ and K^{*0} combinations in the MC sample. We can observe a clear peak corresponding to $B^0 \to J/\psi K^{*0}$. There is also large background contamination. B^0 candidates are selected by calculating the beam energy constrained mass (M_{bc}) and the energy difference between the B^0 candidate and the beam energy (ΔE). The definitions of M_{bc} and ΔE are

$$M_{bc} \equiv \sqrt{E_{beam}^2 - p_{B^0}^2} \quad \text{and} \quad \Delta E \equiv E_{B^0} - E_{beam}, \tag{3.6}$$

where E_{beam} is the beam energy in the center-of-mass frame ($E_{beam} \simeq 5.29$ GeV) and E_{B^0} and p_{B^0} are the energy and momentum of a B^0 candidate in the center-of-mass frame, respectively

The scatter plot of M_{bc} and ΔE for MC sample is shown in Figure 3.5. The beam constrained mass is required to be between 5.27 and 5.29 GeV/c^2. $|\Delta E|$ is required to be less than 30 MeV. These selection criteria correspond to 3σ from the peak. Projections onto M_{bc} and ΔE are also shown in Figure 3.5 with the above requirement on the other axis. Clearly this method yields much better signal to background compared with the invariant mass distribution. When an event has multiple entries in the signal region, we select only one candidate based on

$$\chi^2 = \left(\frac{M_{bc} - 5.28}{\sigma_{M_{bc}}}\right)^2 + \left(\frac{\Delta E}{\sigma_{\Delta E}}\right)^2, \tag{3.7}$$

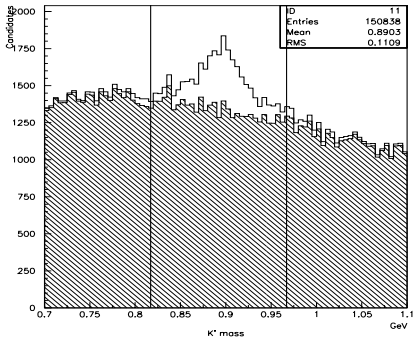

Figure 3.3: Invariant mass distribution for K^{*0} candidates in the MC sample. Hatched area shows the background distribution. Selection criterion is indicated by straight lines.

where $\sigma_{M_{bc}}$ and $\sigma_{\Delta E}$ are the resolutions for M_{bc} and ΔE, respectively. The combination with minimum χ^2 is selected.

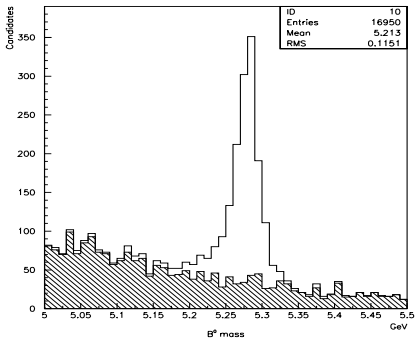

Figure 3.4: The invariant mass distribution of J/ψ and K^{*0} combinations in the MC sample. We can observe a clear peak of B^0. There is also large background contamination.

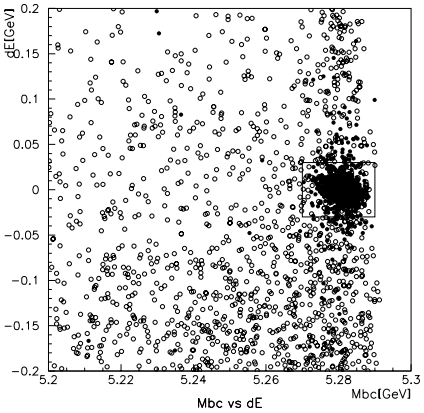

(a) $M_{bc} - \Delta E$

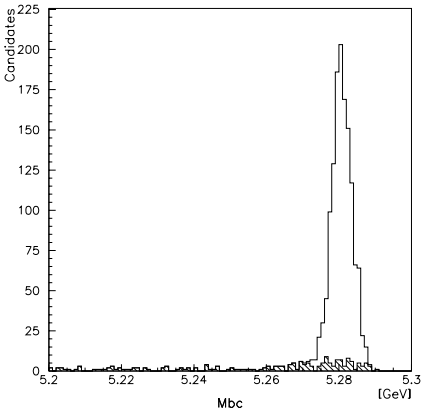

(b) M_{bc}

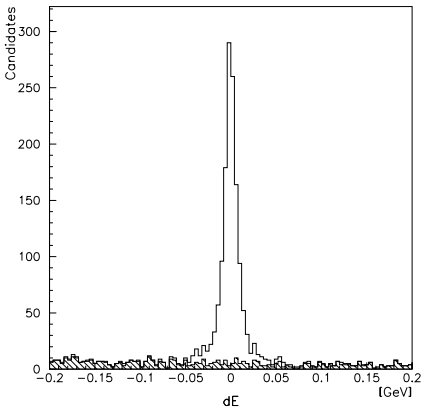

(c) ΔE

Figure 3.5: Scatter plot of M_{bc} vs. ΔE for $B^0 \to J/\psi K^{*0}$ in MC sample. Black circles show signal events and white boxes show background events. The signal region is shown in the box. The projection onto M_{bc} and ΔE are also shown.

3.4 Vertex Reconstruction

The decay vertex of $B^0 \to J/\psi K^{*0}$ is calculated by the vertex constraint fit using the lepton tracks from J/ψ decay. The lifetime of J/ψ is so short that we can neglect the difference between the B^0 decay point and the J/ψ decay point. We require more than or equal to one lepton track to be associated with at least two SVD z hits and one SVD $r\phi$ hit. Interaction point (IP) constraint is applied during the vertex fit to improve the resolution in the $r\phi$ plane.

The average position of the interaction point is calculated for every accelerator fill from the primary vertex position distribution of hadronic events. The size of the interaction region in the horizontal direction (x) is calculated using the primary vertex position distribution; the effect of the primary vertex resolution is deconvoluted in this calculation. The vertex resolution is obtained using the primary vertex position distribution in the vertical direction (y), since the beam size in the direction is less than 10 μm and the σ of the y direction is a good representation of the vertex resolution. The size of the interaction region in the y direction is determined from the average luminosity, the beam current and the x size of the interaction region. The size of the interaction region is typically 100 μm in x and 5 μm in y. Uncertainty of $\sim 20\mu$m is added to the interaction region size to take into account the uncertainty of the B decay position due to the transverse motion of the B meson.

The decay vertex of the associated B, which is called tagging side vertex, is determined using the remaining tracks that are associated with SVD hits in the event. The expected track error in z direction (σ_z^{track}) must be less than 0.5 mm to eliminate badly measured tracks. K_S daughter tracks should be rejected since they do not originate from the B primary vertex. Tracks which can form K_S with any other track are rejected. The K_S daughter tracks are further reduced by eliminating tracks with $\delta z > 1.8$ mm. Here δz is the z distance between the vertex point of the reconstructed B meson and the track position at the closest approach to the reconstructed B vertex. The cut is loose enough not to bias the reconstruction efficiency while effectively rejecting K_S and badly measured tracks. We reject tracks with impact parameter to the interaction point (δr) in $r\phi$ plane greater than 0.5 mm to further reduce the K_S daughter. These cuts, which reject many K_S and badly-measured tracks, are important: if too loose a criterion is used, the fraction of badly-measured events becomes large, and modeling of the resolution becomes difficult.

If the reduced χ^2 ($\chi^2/n \equiv \chi^2/$number of degrees of freedom) of the vertex fit with IP constraint is worse than 20, the track that gives the largest contribution to the χ^2 is removed. This procedure is iterated until the χ^2/n requirement is satisfied or only one track is left. The efficiency to reconstruct the vertex of the associated B meson is 90%. This method does not properly treat the secondary vertex due to charm decay although it tries to reduce the effect by removing tracks which is inconsistent with the decay vertex. The effect of the secondary charm vertex moves the decay vertex point of the associated B toward charm flight direction.

Since we do not know production points of either of B mesons, we cannot

calculate the proper time of either one of two B meson decays. Assuming the B mesons are produced at rest in the $\Upsilon(4S)$ rest frame, the proper time difference Δt is approximated as

$$\Delta t = \frac{1}{c\beta\gamma}(z_{J/\psi K^*} - z_{tag}), \tag{3.8}$$

where $\beta\gamma = 0.425$ at the Belle, $z_{J/\psi K^*}$ is z position of the decay vertex of $B^0 \to J/\psi K^{*0}$ and z_{tag} is z position of the tagging side decay vertex. The distribution for the proper time difference is shown in Figure 3.6.

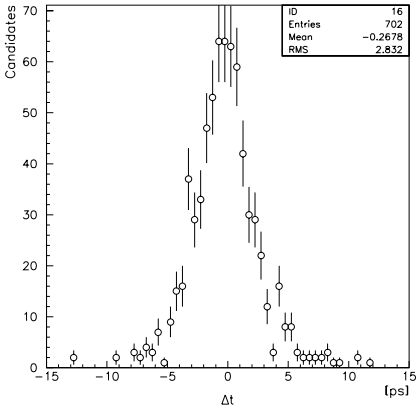

Figure 3.6: The distribution for the reconstructed proper time difference Δt_{rec} in the signal MC sample.

The distribution for the reconstructed proper time difference is deviated from the distribution for the real proper time difference. Figure 3.7 shows the distribution for $\Delta t_{recon} - \Delta t_{gen}$ for the signal MC sample, where Δt_{recon} is Δt reconstructed using the procedure described above and Δt_{gen} is the true Δt, which can be obtained by information from the Monte Carlo event generator. This distribution corresponds to Δt resolution. The resolution function $\mathcal{R}(\Delta t)$ is defined as a sum of two Gaussian to account for its long tail as

$$\begin{aligned} \mathcal{R}(\Delta t) &= \frac{g}{\sqrt{2\pi}\sigma_1} \exp\left(-\frac{(\Delta t - \mu_1)^2}{2\sigma_1^2}\right) \\ &\quad + \frac{1-g}{\sqrt{2\pi}\sigma_2} \exp\left(-\frac{(\Delta t - \mu_2)^2}{2\sigma_2^2}\right). \end{aligned} \tag{3.9}$$

A fit to the $\Delta t_{recon} - \Delta t_{gen}$ distribution yields

The distribution is shifted to negative direction in Δt due to the secondary vertex of the D decay.

g	0.785 ± 0.036
μ_1	-0.184 ± 0.047 ps
σ_1	0.912 ± 0.059 ps
μ_2	0.327 ± 0.334 ps
σ_2	3.72 ± 0.31 ps

Table 3.3: The fit result of the distribution for $\Delta t_{rec} - \Delta t_{gen}$ in the signal MC sample.

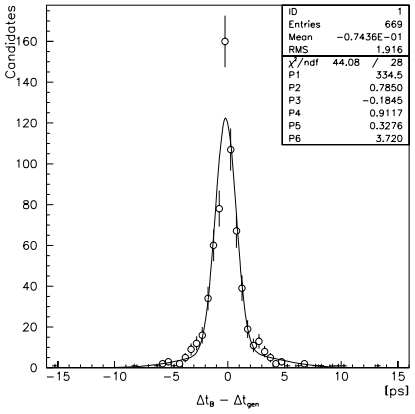

Figure 3.7: The distribution for $\Delta t_{rec} - \Delta t_{gen}$ in the signal MC sample. The fit result with the sum of two Gaussian are indicated by solid curves.

3.5 Flavor Tagging

It is crucial to identify the flavors of the tagging side B mesons, B^0 or $\overline{B}^0$. Our tagging methods are based on the correlation between the flavor of the decaying B^0 mesons and the charge of prompt lepton in $b \to c\nu\ell$ decays (lepton tag), the charge of kaon originating from $b \to c \to s$ decays (kaon tag), or the charge of soft pion from $B \to D^*\ell\nu$, $D^* \to D\pi$ decay chains (soft pion tag). Lepton tag is classified into two categories according to lepton momentum. We applied the following four tagging methods. We tested the event with them in a descending order: if the event failed the method (1), we tested the event with the method (2) and so on.

1. A high momentum lepton: If the tagging side B meson contains a lepton ($\ell^\pm = e^\pm$ or $\mu^\pm$) with momentum $p^* \geq 1.1$ GeV/c^2 in the center-of-mass frame, we assign $f_{tag} = B^0(\overline{B}^0)$ for $\ell^+(\ell^-)$, where f_{tag} is the flavor of the tagging side B. First, electron is examined. When two or more high momentum electrons are found, no flavor is assigned. If the flavor is not

determined by electron, muon is examined. Again, no flavor is assigned for two or more high momentum muons.

2. A charged kaon: If the tagging side B meson contains no high momentum lepton, the sum of the charges of all identified kaons, Q_K, in the tagging side B is investigated. We assign $f_{tag} = B^0(\overline{B}^0)$ for $Q_K > 0 (Q_K < 0)$. If $Q_K = 0$, the event fails this method.

3. A medium momentum lepton: If the tagging side B meson contains the lepton with momentum 0.6 GeV/$c^2 \leq p^* \leq$ 1.1 GeV/c^2 in the center-of-mass frame, we calculate the center-of-mass missing momentum (p^*_{miss}) as a approximation of the ν center-of-mass momentum. The medium momentum lepton can be originated from the charm quark decay. Its charge are opposite to the estimated charge. In order to reject such leptons, we impose the condition $p^*_\ell + p^*_{miss} \geq 2.0$GeV/$c$. If the condition is satisfied, we assume that the lepton is from $b \to c\nu\ell$ decay and assign f_{tag} based on the charge of ℓ as in the method (1).

4. A soft pion: If the tagging side B meson contains a low momentum ($p^* <$ 200 MeV/c) charged track consistent with π of $D^* \to D\pi$ decay, we assign $f_{tag} = B^0(\overline{B}^0)$ for $\pi^-(\pi^+)$.

If we can identify the flavor of the tagging side B meson for N_{tag} candidates among N reconstructed events, the tagging efficiency (ϵ) and its uncertainty are defined as

$$\epsilon \equiv \frac{N_{tag}}{N}, \tag{3.10}$$

$$\sigma_\epsilon \equiv \frac{1}{N}\sqrt{\frac{N_{tag}(N - N_{tag})}{N}}. \tag{3.11}$$

The probability to misidentify the flavor (wrong tag fraction, w) is defined as

$$w \equiv \frac{N_{mis}}{N_{tag}}, \tag{3.12}$$

$$\sigma_w \equiv \frac{1}{N_{tag}}\sqrt{\frac{N_{mis}(N_{tag} - N_{mis})}{N_{tag}}}, \tag{3.13}$$

where N_{mis} is the number of misidentified events out of N_{tag} events of tagged candidates. The wrong tag fraction can be calculated using the information from the Monte Carlo event generator. The tagging efficiency (ϵ) and the wrong tag fraction(w) found in the signal MC sample are tabulated in Table 3.4. The wrong tag fraction obtained for each tagging method in this analysis is used in the Δm_d fit as described below.

Tagging method	ϵ	w
High $p^*\ell$	0.160 ± 0.011	0.087 ± 0.046
$K^\pm$	0.303 ± 0.013	0.161 ± 0.029
Med $p^* e^\pm$	0.016 ± 0.004	0.269 ± 0.147
Med $p^* \mu^\pm$	0.014 ± 0.004	0.315 ± 0.164
Soft pion	0.077 ± 0.008	0.341 ± 0.073

Table 3.4: The tagging efficiency (ϵ) and the wrong tag fraction (w)

3.6 Δm_d Fit to Signal Events

Δm_d is extracted from the distribution of the proper time difference Δt of two B decays using an unbinned maximum likelihood fit. We study the fit function for the signal using the signal MC sample in this section.

The probability to observe opposite flavor (OF) or same flavor (SF) is given by

$$P_{OF}(\Delta t) = \frac{1}{4\tau_{B^0}} \exp\left(-\frac{|\Delta t|}{\tau_{B^0}}\right)[1+\cos(\Delta m_d \Delta t)], \quad (3.14)$$

$$P_{SF}(\Delta t) = \frac{1}{4\tau_{B^0}} \exp\left(-\frac{|\Delta t|}{\tau_{B^0}}\right)[1-\cos(\Delta m_d \Delta t)], \quad (3.15)$$

where τ_{B^0} is B^0 lifetime. Observed OF or SF states actually contain both OF and SF states according to the wrong tag fraction w as

$$P_{OF} \rightarrow (1-w)P_{OF} + wP_{SF} \propto 1 + (1-2w)\cos(\Delta m_d \Delta t), \quad (3.16)$$

$$P_{SF} \rightarrow wP_{OF} + (1-w)P_{SF} \propto 1 - (1-2w)\cos(\Delta m_d \Delta t). \quad (3.17)$$

In addition, the Δt distribution is smeared by the Δt resolution function, $\mathcal{R}(\Delta t)$, as described in section 3.4. Taking into account those effects, the likelihood function for the signal events is defined as

$$\mathcal{L}(\Delta m_d) = \prod_i \mathcal{P}^i_{OF}(\Delta t_i, \Delta m_d) \prod_j \mathcal{P}^j_{SF}(\Delta t_j, \Delta m_d), \quad (3.18)$$

$$\mathcal{P}^i_{OF}(\Delta t, \Delta m_d) = \int_{-\infty}^{\infty} dt' \frac{1}{4\tau_{B^0}} \exp\left(-\frac{|t'|}{\tau_{B^0}}\right) [1+(1-2w)\cos(\Delta m_d t')] \cdot \mathcal{R}(\Delta t - t'),$$

$$\mathcal{P}^j_{SF}(\Delta t, \Delta m_d) = \int_{-\infty}^{\infty} dt' \frac{1}{4\tau_{B^0}} \exp\left(-\frac{|t'|}{\tau_{B^0}}\right) [1-(1-2w)\cos(\Delta m_d t')] \cdot \mathcal{R}(\Delta t - t'),$$

$$\mathcal{R}(\Delta t) = \frac{g}{\sqrt{2\pi}\sigma_1} \exp\left(-\frac{(\Delta t - \mu_1)^2}{2\sigma_1^2}\right) + \frac{1-g}{\sqrt{2\pi}\sigma_2} \exp\left(-\frac{(\Delta t - \mu_2)^2}{2\sigma_2^2}\right),$$

where i runs over the opposite flavor events and j runs over the same flavor events. An appropriate wrong tag fraction is chosen for each event according to the tagging method for the event. Δm_d is fit to maximize the likelihood function for the signal MC sample. The fit yields

$$\Delta m_d = 0.460 \pm 0.043 \text{ ps}^{-1}, \tag{3.19}$$

which is consistent with $\Delta m_d = 0.423$ ps^{-1} used for the MC production. The Δt distributions for OF and SF events in the signal MC sample are shown in Figure 3.8. Fit results are also superimposed. From (3.14) and (3.15), we define opposite-to-same flavor asymmetry A_{chg} as

$$A_{chg}(\Delta t) = \frac{N_{OF} - N_{SF}}{N_{OF} + N_{SF}} = \frac{P_{OF} - P_{SF}}{P_{OF} + P_{SF}} \propto \cos(\Delta m_d \Delta t). \tag{3.20}$$

A_{chg} as a function of Δt is shown in Figure 3.9.

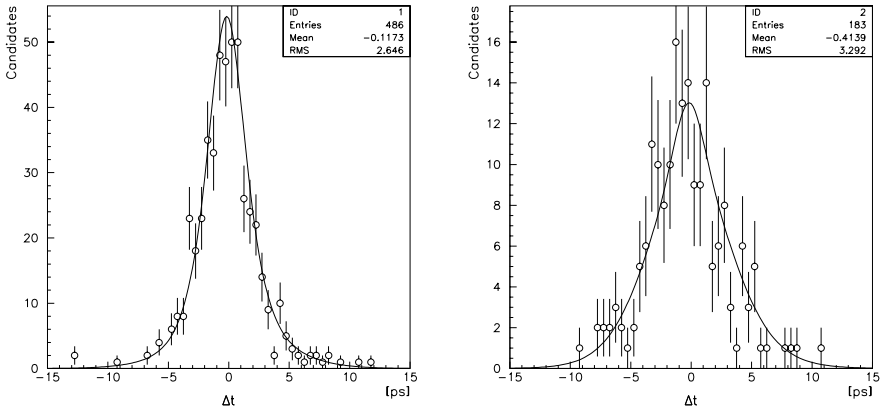

(a) Δt distribution for the opposite flavor events

(b) Δt distribution for the same flavor events

Figure 3.8: The Δt distribution for (a) the opposite flavor and (b) the same flavor events in the signal MC sample. The points represent the Δt distributions in the signal MC sample. Solid line represents the Δm_d fit result.

3.7 Δm_d Fit with Background

Taking into account the effect of the background contribution, the likelihood function is defined as:

$$\mathcal{L}(\Delta m_d) \quad = \quad \prod_i [(1 - f_{BG}^{OF})\mathcal{P}_{OF}^i(\Delta t_i) + f_{BG}^{OF}\mathcal{P}_{BG(OF)}^i(\Delta t_i)]$$

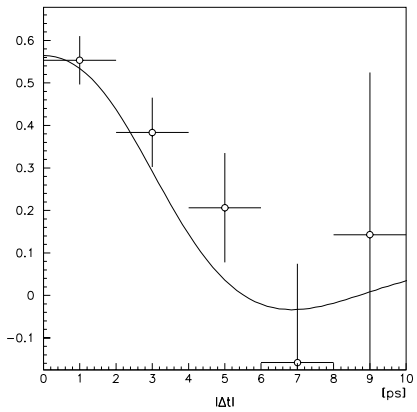

Figure 3.9: A_{chg} as a function of Δt in the signal MC sample. Points are calculated from observed events. Smooth curve is obtained from the result of the fit.

$$\prod_j [(1 - f_{BG}^{SF})\mathcal{P}_{SF}^i(\Delta t_j) + f_{BG}^{SF}\mathcal{P}_{BG(SF)}^j(\Delta t_j)], \quad (3.21)$$

$$\mathcal{P}_{OF}^i(\Delta t, \Delta m_d) = \int_{-\infty}^{\infty} dt' \frac{1}{4\tau_{B^0}} \exp\left(-\frac{|t'|}{\tau_{B^0}}\right) [1 + (1-2w)\cos(\Delta m_d t')] \cdot \mathcal{R}(\Delta t - t'),$$

$$\mathcal{P}_{SF}^j(\Delta t, \Delta m_d) = \int_{-\infty}^{\infty} dt' \frac{1}{4\tau_{B^0}} \exp\left(-\frac{|\Delta t'|}{\tau_{B^0}}\right) [1 - (1-2w)\cos(\Delta m_d t')] \cdot \mathcal{R}(\Delta t - t'),$$

where i runs over the opposite flavor events in the signal region, j runs over the same flavor events in the signal region. f_{BG}^{OF} and f_{BG}^{SF} are the background fractions for the opposite and the same flavor events, which are calculated for each event based on the ΔE distributions. $\mathcal{P}_{BG(OF)}^i(\Delta t)$ and $\mathcal{P}_{BG(SF)}^i(\Delta t)$ are the probability density functions for the corresponding backgrounds. They are described in the following subsections.

3.7.1 Background Fraction

The background fraction is calculated event by event from the ΔE distribution because feed across from the $B \to J/\psi X$ decays is the dominant background contribution. M_{bc} distribution from those backgrounds is similar to signal, and it is not suitable to calculate the background fraction. ΔE distribution of the MC sample is fit with a sum of two Gaussians for the signal and a first order

polynomial for the background;

$$\begin{aligned} F_{SIG}(\Delta E) &= A \cdot \left[\frac{1-f_{tail}}{\sqrt{2\pi}\sigma} \exp\left(-\frac{(\Delta E-\mu)^2}{2\sigma^2} \right) \right. \\ &\quad \left. + \frac{f_{tail}}{\sqrt{2\pi}\sigma_{tail}} \exp\left(-\frac{(\Delta E-\mu_{tail})^2}{2\sigma_{tail}^2} \right) \right], \\ F_{BG}(\Delta E) &= B_0 \cdot (1 + B_1 \cdot \Delta E), \end{aligned}$$

where $F_{SIG}(\Delta E)$ and $F_{BG}(\Delta E)$ are the signal and background functions. Using the ΔE functions for signal and background events, the background fraction $f_{BG}(\Delta E)$ is defined as

$$f_{BG}(\Delta E) = \frac{F_{BG}(\Delta E)}{F_{BG}(\Delta E) + F_{SIG}(\Delta E)}. \tag{3.22}$$

Since the background contribution may be different between OF and SF states, we should use different background fraction functions for OF and SF states. We fit the ΔE distributions for OF and SF events separately to obtain those background fraction functions. Figure 3.10 shows the ΔE distributions for OF and SF events and fit results. The fit results are tabulated in Table 3.5.

Parameter	Opposite Flavor	Same Flavor
A	1.27±0.14	0.583±0.069
μ	-0.00027±0.0004	-0.0010±0.0005
σ	0.00531±0.00039	0.00665±0.00051
f_{tail}	0.438±0.086	0.398±0.128
σ_{tail}	-0.0021±0.0016	0.014±0.014
μ_{tail}	0.0187±0.0014	0.072±0.14
B_0	1.11±0.07	0.358±0.049
B_1	-2.69±0.23	-2.90±0.53

Table 3.5: The fit result of the ΔE distributions for the opposite flavor and same flavor background events. μ and σ have a unit in GeV. B_1 has a unit in GeV^{-1}

3.7.2 Background Probability Density Function

The Δt distribution of the background events depend on the source of the backgrounds. The backgrounds from $B\overline{B}$ and continuum events are considered. The Δt distribution of the continuum events appears to have no lifetime since all tracks come from the interaction point, while that of the $B\overline{B}$ events has lifetime. The distribution is convoluted with a resolution function. The probability density function for the background events is defined as

$$\mathcal{P}_{BG}^{k}(\Delta t, f_{BG}^{0}) = \int_{-\infty}^{\infty} dt' \mathcal{R}_{BG}(\Delta t - t')$$

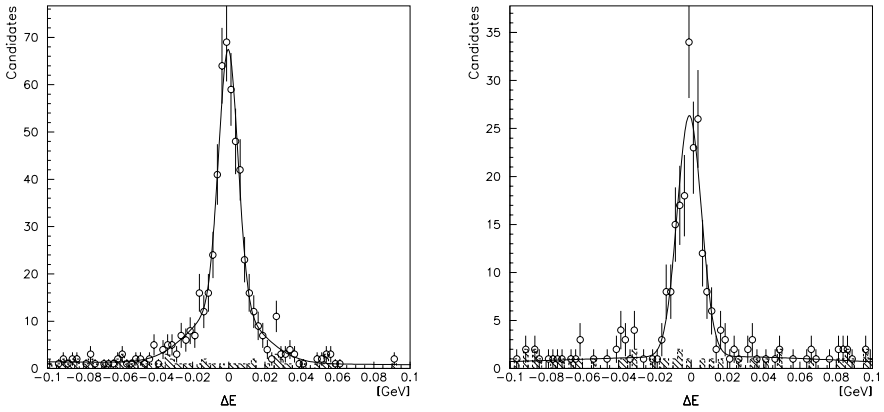

(a) OF (b) SF

Figure 3.10: The ΔE distributions for (a) the opposite flavor and (b) the same flavor background events in the MC sample. The points represent the ΔE distribution. Solid lines represent the fit results. Dotted lines show the background contributions.

$$\left\{ f^0_{BG}\delta(t') + \frac{1-f^0_{BG}}{2\tau_{BG}} \exp\left(-\frac{|t'|}{\tau_{BG}}\right) \right\}, \quad (3.23)$$

$$\mathcal{R}_{BG}(\Delta t, \mu_{BG}, \sigma_{BG}) = \frac{1}{\sqrt{2\pi}\sigma_{BG}} \exp\left(-\frac{(\Delta t - \mu_{BG})^2}{2\sigma^2_{BG}}\right).$$

Resolution function is represented by a Gaussian instead of a sum of two Gaussians due to poor statistics of the background sample. A likelihood fit is performed for the background sample of the opposite flavor and the same flavor in the sideband region of the $M_{bc} - \Delta E$ distribution using the MC sample. The Δt distribution and the fit result are shown in Figure 3.11. The fit results are summarized in Table 3.6. The parameters obtained here are used for the Δm_d fit in the following subsection.

Flavor	Opposite	Same
τ_{BG} [ps]	2.21 ± 0.71	2.35 ± 0.90
f^0_{BG}	0.745 ± 0.187	0.682 ± 0.268
μ_{BG} [ps]	-0.301 ± 0.114	-0.390 ± 0.160
σ_{BG} [ps]	1.77 ± 0.18	2.06 ± 0.25

Table 3.6: Fit results for the background events in the MC sample.

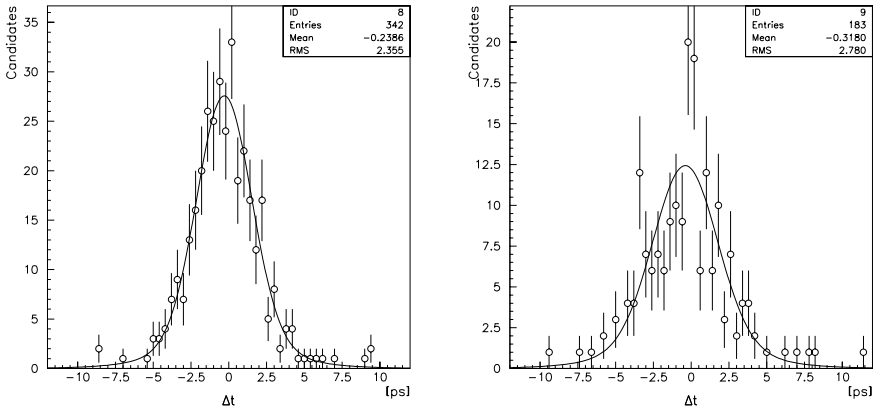

(a) OF (b) SF

Figure 3.11: The Δt distribution for (a) the opposite flavor and (b) the same flavor background events in the MC sample. The points represent the reconstructed Δt. Solid line represents the fit results.

3.7.3 Fit Result for MC Sample with Background

Using the likelihood function described in equation (3.21), (3.22) and (3.23), we perform an unbinned maximum likelihood fit to extract the Δm_d using the events in the signal region of the MC sample. The fit gives

$$\Delta m_d = 0.461 \pm 0.043 \text{ ps}^{-1}. \tag{3.24}$$

This result is consistent with the value $\Delta m_d = 0.423$ ps^{-1} used in the MC event generator. The Δt distributions for OF and SF events in the signal region of the MC sample are shown along with the fit results in Figure 3.12. A_{chg} as a function of the Δt is shown in Figure 3.13.

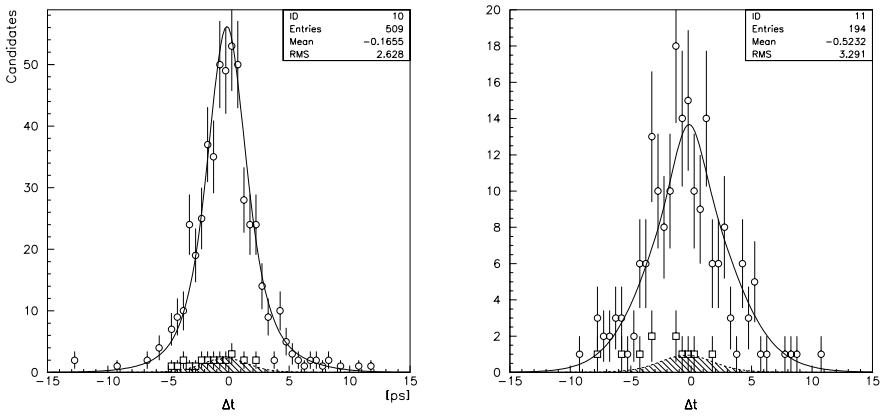

(a) Δt distribution for the opposite flavor events

(b) Δt distribution for the same flavor events

Figure 3.12: The Δt distributions for (a) the opposite flavor and (b) the same flavor events in the MC sample with background. The circle points represent the proper time difference distribution in the signal region. The square points represent the proper time difference distribution for the background in the signal region. Solid line represents the Δm_d fit results. Doted line represents the background component of the Δm_d fit.

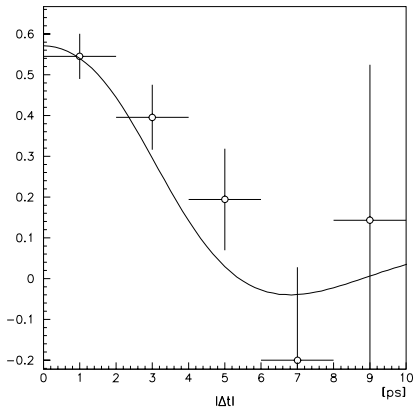

Figure 3.13: A_{chg} as a function of the Δt in the MC sample with background. Points are calculated from observed events. Smooth curve is obtained from the result of the fit.

Chapter 4

Data Analysis

In this chapter, we analyze 5.8fb^{-1} of experimental data collected with the Belle detector.

4.1 Reconstruction

The selection criteria of the candidate for the data are the same as those for the MC sample described in the previous chapter. The invariant mass distribution for J/ψ and K^{*0} are shown in Figure 4.1 and Figure 4.2, respectively. The scatter plot of M_{bc} - ΔE for $B^0 \to J/\psi K^{*0}$ is shown in Figure 4.3. The signal region is defined to be 5.27 GeV/c^2 $< M_{bc} <$ 5.29 GeV/c^2 and -0.03 GeV $< \Delta E < 0.03$ GeV. The Δt is also calculated by the procedure described in the previous chapter. The distribution for Δt is shown in Figure 4.4.

4.2 Δm_d Fit

The oscillation frequency Δm_d is extracted from the data by performing an unbinned maximum likelihood fit to the Δt distribution. The likelihood function defined in the previous chapter is used. The parameters for the resolution function and the background functions are derived in the following subsections.

4.2.1 Resolution Function

Since statistics is too poor to determine the resolution function from $B^0 \to J/\psi K^{*0}$ sample, we use $B \to D^* \ell \nu$ events to determine the resolution function. Since the Δt resolution is dominated by the resolution of tagging side vertex, the difference of the resolution function between $B^0 \to J/\psi K^*$ and $B \to D^* \ell \nu$ samples is considered to be negligible. The resolution function described in the previous chapter is used in the fit. The parameters in the resolution function are tabulated in Table 4.1.

g	0.773 ± 0.015
μ_1	-0.148 ± 0.012ps
σ_1	0.852 ± 0.015ps
μ_2	-0.321 ± 0.055ps
σ_2	2.31 ± 0.06ps

Table 4.1: Parameters in the resolution function

4.2.2 Background Function

The background fraction $f_{bkg}(\Delta E)$ in the signal region is estimated from the distribution of ΔE, as discussed in the previous chapter. Due to the poor statistics, the ΔE distribution is fit with a Gaussian for the signal and a constant term for the background:

$$\begin{aligned} F_{SIG}(\Delta E) &= \frac{A}{\sqrt{2\pi}\sigma} \exp\left(-\frac{(\Delta E - \mu)^2}{2\sigma^2}\right) \\ F_{BG}(\Delta E) &= B_0 \end{aligned}$$

where F_{SIG} and F_{BG} are the signal and background functions. Figure 4.5 shows the ΔE distribution in the data and the fit result. The fit result for the ΔE distribution is tabulated in Table 4.2.

Parameter	Opposite Flavor	Same Flavor
A	0.0769±0.0131	0.0374±0.0087
μ	-0.00040±0.0015	-0.0029±0.000513
σ	0.00837±0.00140	0.00554±0.00092
B_0	0.128±0.027	0.021±0.011

Table 4.2: Fit result for the ΔE distribution in the data. μ and σ have a unit in GeV.

The statistics in the real data is too poor to determine the Δt distribution for the background events. We use the parameters for the background probability density function obtained using the MC sample as described in the previous chapter. Since the background fraction is very small, the effect of the uncertainty of the background probability density function is expected to be small.

4.2.3 Flavor Tagging

The flavor of the tagging side B meson is determined by the procedure described in the previous chapter. The tagging efficiency (ϵ) for the data sample is tabulated in Table 4.3. The wrong tag fraction obtained using the MC sample is used for the data fit.

Tagging method	ϵ
High $p^*\ell$	0.139 ± 0.031
$K^\pm$	0.270 ± 0.040
Med $p^*e^\pm$	0.016 ± 0.011
Med $p^*\mu^\pm$	0.008 ± 0.008
Soft pion	0.074 ± 0.024

Table 4.3: The tagging efficiency (ϵ) for each tagging method.

4.2.4 Fit Result

Δm_d is extracted by an unbinned maximum likelihood fit to the Δt distribution for the $B^0 \to J/\psi K^*$ sample in the data. The likelihood function described in the previous chapter is used in the fit. The parameter for the likelihood function is determined using the data as described in the previous subsections. The Δm_d is obtained as

$$\Delta m_d = 0.591 \pm 0.141 \text{ps}^{-1}. \tag{4.1}$$

The value is consistent with the world average value of $\Delta m_d = 0.472 \pm 0.017 \text{ps}^{-1}$[3] within one standard deviation. The Δt distribution and fit result for the data are shown in Figure 4.6. A_{chg} as a function of Δt is shown in Figure 4.7.

4.2.5 Systematic Uncertainties

We examine the following systematic effects.

- Resolution function: The parameters for the resolution function (g, μ_1, σ_1, μ_2 and σ_2) have been varied by $\pm 1\sigma$. The changes in the fit results are estimated to be systematic errors. All errors are added in quadrature.

- Background fraction: As described in Section 4.7, the background fraction f_{BG}^{OF} and f_{BG}^{SF} are determined based on the fits to the ΔE distributions in the data. The associated systematic error is estimated by varying the parameters to determine f_{BG}^{OF} and f_{BG}^{SF} (A, μ, σ and B_0) by $\pm 1\sigma$. In addition, systematic error associated with the choice of the parameterization is studied. The ΔE distribution of the background is represented by a constant term for the data while first order polynomial is used for the MC. The first order polynomial is used for the data using the slope obtained from the MC sample to estimated the error due to the difference in the background function.

- Background shape: Since probability density function for the background is determined using the MC sample, uncertainties and imperfections in the Monte Carlo simulation lead to systematic errors in the background distributions. The associated systematic error is estimated by varying the parameters (τ_{BG}, f_{BG}^0, μ_{BG} and σ_{BG}) by two standard deviation.

- Wrong tag fraction: The wrong tag fraction for each tagging method is varied by two standard deviation to estimate the error associated with the error of the wrong tag fraction since the wrong tag fractions are obtained using the MC sample.

Contributions to the systematic error are summarized in Table 4.4. The contribution from the wrong tag fraction is dominant. Total systematic error is obtained by adding all contributions quadratically.

Source(uncertainty)	systematic error
Resolution function	$\pm$ 0.004
Background fraction	$< \pm$ 0.001
Background shape	$< \pm$ 0.001
Wrong tag fraction	$^{+0.053}_{-0.112}$
total	$^{+0.054}_{-0.112}$

Table 4.4: Summary of systematic error.

4.3 Discussion

Combining the fit result and systematic error, we obtain

$$\Delta m_d = 0.591 \pm 0.141(\text{stat})^{+0.054}_{-0.112}(\text{sys})\ \text{ps}^{-1}$$

The result is consistent with the world average value $\Delta m_d = 0.472 \pm 0.017\ \text{ps}^{-1}$ within one standard deviation. However, both statistical error and systematic error are very large. There is room for improvement in the analysis of this paper.

Statistical error is larger than systematic error. We can improve the precision of the measurement of Δm_d by taking more data. In addition, we plan to measure Δm_d of other modes: $B^0 \to D^{*-}\ell^+\nu_\ell$, $B^0 \to D^{*-}\rho^+$, $B^0 \to D^-\pi^+$, and so on.

In order to improve the precision of the measurement of Δm_d, we need to suppress the systematic error. As shown in the Table 4.4, the systematic error originating from the wrong tag fraction is the most contributed to the systematic error. We need more precise measurement of the flavor of the tagging side B. More statistics will make us determine the wrong tag fractions from the real data. It is estimated that systematic error will be much smaller, while statistical error will be a little larger.

The mass difference Δm_d can be represented by the CKM matrix element, V_{td}, as shown in (1.11),

$$\Delta m_d = \frac{G_F^2}{6\pi^2}|V_{td}V_{tb}^*|^2 m_t^2 m_{B_d} f_B^2 B_B \eta_{QCD} F\left(\frac{m_t^2}{m_W^2}\right).$$

Using the QCD calculation results, we can estimate the the value of $|V_{td}|$ with some uncertainty. From the QCD calculations and experimental results, we have the next-to-leading-order QCD corrections $\eta_{QCD} = 0.55$, the running top-quark mass $m_t = 166 \pm 5\mathrm{GeV}/c^2$, $f_B^2 B_B = (210 \pm 40\mathrm{MeV})^2$, $m_W = 80.41\mathrm{GeV}/c^2$ and $G_F/(\hbar c)^3 = 1.166 \times 10^{-5}\mathrm{GeV}^{-2}$ [3]. $F(x)$, which represents the decay constant for B mesons, is given by

$$F(x) = \frac{4 - 11x + x^2}{4(1-x)^2} - \frac{3x^2 \ln x}{2(1-x)^3}.$$

Then we obtain

$$|V_{tb}^* V_{td}| = 0.0093 \pm 0.0018^{+0.0015}_{-0.0020},$$

where the first error is originated from the uncertainty of m_t and $f_B^2 B_B$, and the second error is originated from the uncertainty of V_{td}. Estimated errors are combined in quadrature. Using the experimental constraints together with unitarity, the 90% confidence limits on the magnitude of V_{tb} is

$$|V_{tb}| = 0.9990 \sim 0.9993.$$

Then

$$|V_{tb}| = 0.0093 \pm 0.0018^{+0.0015}_{-0.0020}.$$

The result is consistent with the value which is derived from the world average value: $|V_{td}| = 0.0083 \pm 0.0016$, within one standard deviation.

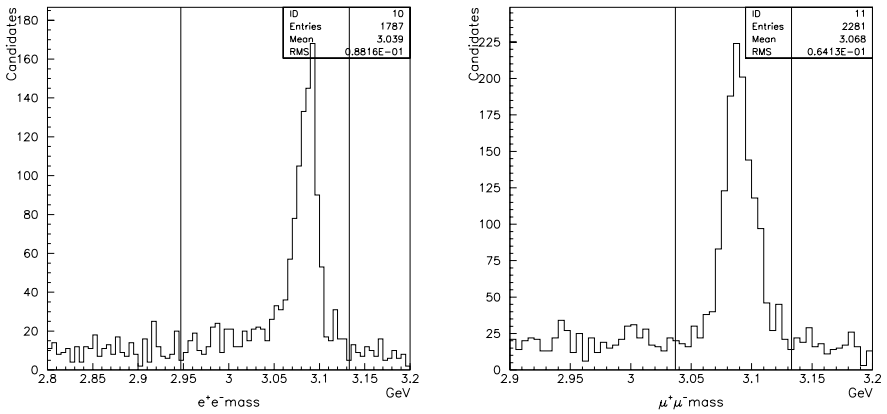

(a) $J/\psi \to e^+e^-$ (b) $J/\psi \to \mu^+\mu^-$

Figure 4.1: Invariant mass distributions for J/ψ candidates. Selection criteria are indicated by straight lines.

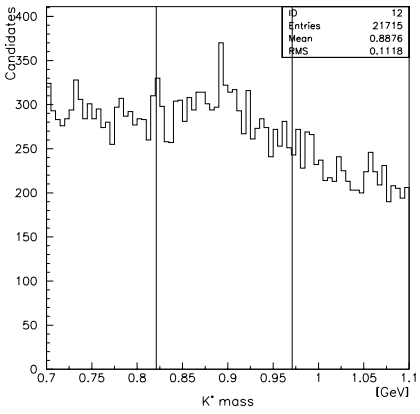

Figure 4.2: Invariant mass distribution for K^{*0} candidates. Selection criterion is indicated by straight lines.

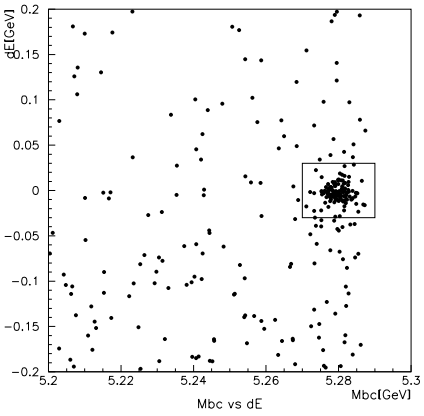

(a) $M_{bc} - \Delta E$

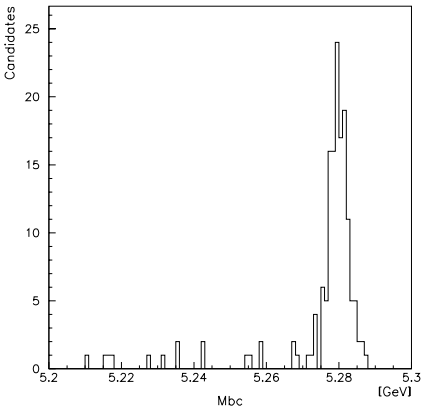

(b) M_{bc}

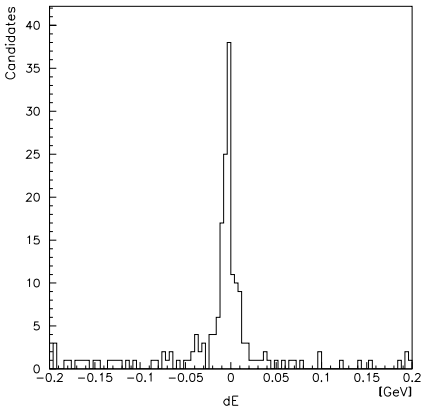

(c) ΔE

Figure 4.3: Scatter plot of M_{bc} vs. ΔE for $B^0 \to J/\psi K^{*0}$ events in the data. The signal region is shown in the box. The projections onto M_{bc} and ΔE axes are also shown.

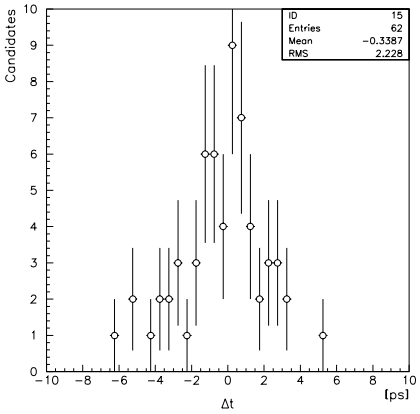

Figure 4.4: The distribution for the proper time difference Δt.

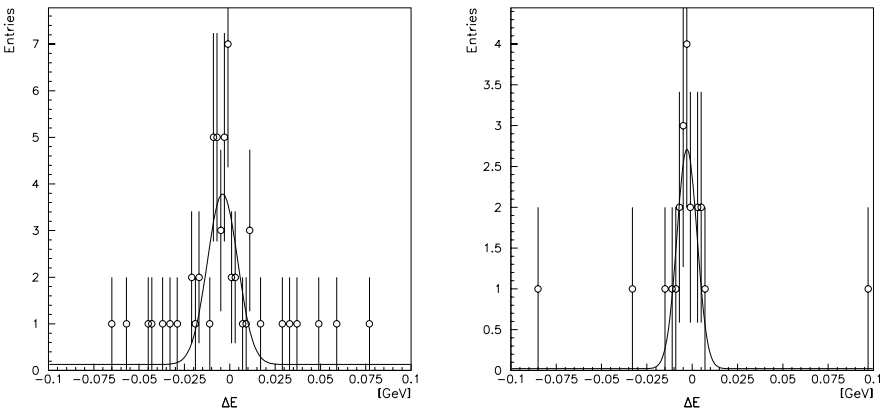

(a) OF (b) SF

Figure 4.5: The ΔE distribution for (a) the opposite flavor and (b) the same flavor events in the data. The points represent the data. Solid lines represent the fit results.

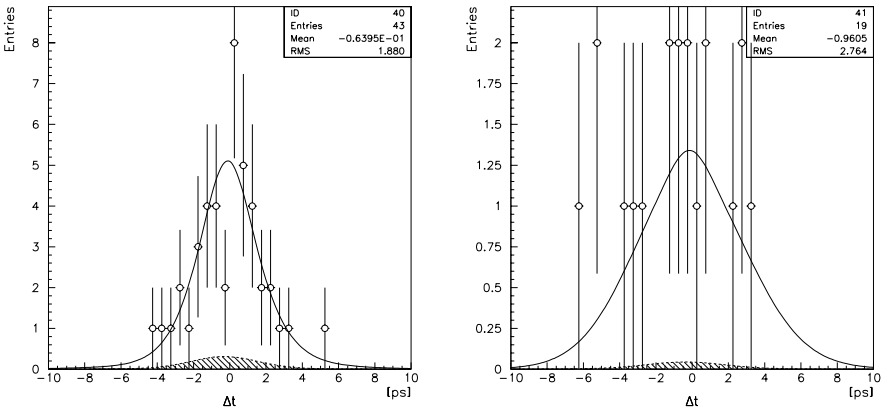

(a) OF (b) SF

Figure 4.6: The Δt distribution for (a) the opposite flavor and (b) the same flavor events in the data. Circle points show data. Solid lines show the results of the Δm_d fit. Dotted lines show the background component of the fit.

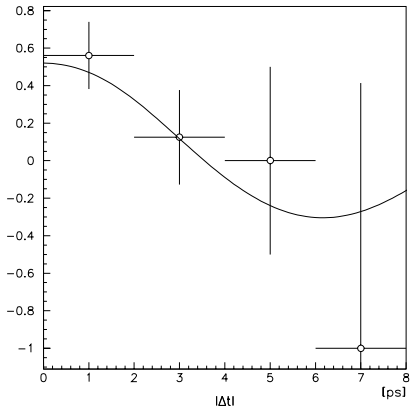

Figure 4.7: A_{chg} as a function of Δt for the data. Points are calculated from observed events. Smooth curve is obtained from the result of the fit.

Chapter 5

Conclusion

We have measured the B^0_d-$\overline{B}^0_d$ oscillation frequency Δm_d from the time evolution of B^0_d-$\overline{B}^0_d$ mixing using the $B^0 \to J/\psi K^{*0}$ decay in a sample comprising 5.8 fb^{-1} of data. An unbinned maximum likelihood fit to proper time difference distributions for the opposite and same flavor events yields

$$\Delta m_d = 0.591 \pm 0.141(\text{stat})^{+0.054}_{-0.112}(\text{sys}) \text{ ps}^{-1}$$

The result is consistent with the world average value $\Delta m_d = 0.472 \pm 0.017$ ps^{-1} within one standard deviation. It demonstrates the capability of measuring time evolution of B^0_d-$\overline{B}^0_d$ mixing at an asymmetric e^+e^- collider at the $\Upsilon(4S)$, which is essential for the measurement of indirect CP asymmetries.

Acknowledgments

I wish to express my great thank to my Supervisor H.Aihara for his excellent advice. I am also specially thankful to H.Tajima for his powerful support in my studies. I greatly acknowledge the Belle group for their support. I appreciate all the members of our lab, J.Tanaka, M Yokoyama, T.Higuchi, T.Nakadaira, T.Tomura, and H.Kawai.

Bibliography

[1] Belle collaboration. A study of CP violation in b meson decays - technical design report. Technical Report 1, KEK, 1995.

[2] A.Abashian *et al.* Measurement of $B^0_d - \overline{B^0_d}$ mixing rate from the time evolution of dilepton events at the Υ(4S). *submitted to Phys.Rev.Lett.*

[3] Particle Data Group. Review of particle physics. *The European Physical Journal C*, 3(14):1-794, 2000.

[4] Hiroaki Aihara. A measurement of CP violation in B^0 meson decays with belle. *hep-ex/0010008.*

[5] Jun-ichi Suzuki. Measurement of B^0_d-$\overline{B}^0_d$ oscillation frequency Δm_d and Wrong flavor tag fraction using $B^0 \to D^{(*-)}\ell\nu$. *BELLE note* #313.

[6] T.Kawasaki, M Hazumi. Tag-side Vertex Reconstruction. *BELLE note* #314.